Construction and Building Materials 174 (2018) 684–692

Contents lists available at ScienceDirect

Construction and Building Materials

journal homepage: www.elsevier.com/locate/conbuildmat

Relationship between flexural strength and pore structure of pavement concrete under fatigue loads and Freeze-thaw interaction in seasonal frozen regions

Aiqin Shen, Senlin Lin *, Yinchuan Guo, Tianqin He, Zhenghua Lyu

Key Laboratory for Special Region Highway Engineering of Ministry of Education, Chang'an University, Xi'an 710064, Shaanxi, China

HIGHLIGHTS

- Interaction function of fatigue load and freeze–thaw on pore-structure is investigated.
- The properties of pore-structure and flexural strength are studied.
- Interaction effect accelerates the deterioration rate of the pore-structure.
- The relationship between flexural strength and pore structure is analyzed using gray relational analysis.

ARTICLE INFO

Article history:
Received 2 January 2018
Received in revised form 9 April 2018
Accepted 21 April 2018

Keywords:
Concrete pavement
Fatigue load
Freeze-thaw
Interaction
Pore structure
Flexural strength
Gray relational analysis

ABSTRACT

To explore the correlation between the flexural strength decay and the pore structure evolution of pavement concrete in seasonal frozen regions, 4 stages of an interaction experimental scheme were designed. The characteristic parameters of pore structure under the interactions were quantitatively characterized, and the correlation between the flexural strength decay and the microstructure evolution was discussed. The results show that the flexural strength of concrete under this interaction presents a parabolic attenuation trend. The specific surface area, the most probable aperture and the less harmful pores were the most important microstructure parameters affecting the flexural strength of concrete; their gray correlations were 0.8 or greater. Further, the regression analysis shows that there is a good linear relationship between the flexural strength attenuation and the pore structure evolution; the regression coefficient reaches 0.845.

1. Introduction

Pavement concrete undergoes fatigue load and freeze–thaw interaction in seasonal frozen regions, accelerating the deterioration rate of the concrete structure [1,2]. The performance and durability of pavement concrete will deteriorate due to microstructural damage occurring in the early stage of life [3,4]. As a result, the development and application of concrete pavement were restricted in seasonal frozen regions [5]. Pavement concrete is a porous material, and the strength of the concrete was affected directly by the internal pore structure. The pore structure deterioration was the attenuation mechanism of flexural strength [6–8].

Omkar et al. compared the pore structure of concrete before and after fatigue load, and they concluded that an increase in pore volume fraction by approximately 10% resulted in a reduction in the compressive strength by approximately 50% [9]. Zhang et al. determined that the pore grading transferred from a smaller pore to a larger pore by studying the structure of concrete pores under the action of the freeze–thaw cycle [10]. Park et al. found that the long-term strength loss of concrete was caused by an increase in the total porosity and amounts of smaller pores in the material [11]. Some other literature showed that the loss of long-term strength is induced by an increase in porosity and an increased incidence of microcracking in cement paste [12,13]. On the other hand, some research has been conducted on the correlation between the macroscopic properties of concrete and its pore structure. Ozturk et al. established the relationship between concrete strength and porosity by regression analysis of a large number of experimental data [14]. Older et al. studied the strength and pore structure of concrete with different water-cement ratios and established a model of the relationship between strength and pore size

* Corresponding author.
E-mail address: lsl421357732@163.com (S. Lin).

https://doi.org/10.1016/j.conbuildmat.2018.04.165
0950-0618/

distribution using a linear regression method [15]. Kumar et al. introduced the average pore size to establish the relationship between the concrete strength and pore structure based on the porosity [16]. Zhou et al. found that there was a good linear correlation between porosity parameters and strength [17]. Jin SS et al. established a multivariate model of the fractal dimension and strength of concrete through regression analysis [18].

Therefore, a considerable amount of research has been reported on concrete strength and pore structure. However, the current studies mainly focus on the compressive strength of the concrete and the effect of a single environmental factor on the concrete. The deterioration of the flexural strength of pavement concrete was more important than the compressive strength [19]. The pavement concrete in seasonal frozen regions is subject to load fatigue and freeze–thaw cycles, causing pore damage and attenuation of flexural strength [20]. Little studies involve the external environment that cannot reflect the true relationship between the pore structure and pavement concrete strength.

This paper aims to determine the relationship between the pore structure of pavement concrete and its flexural strength under the interaction of fatigue load and the freeze–thaw cycle. Furthermore, the gray relational method was used to analyze the pore structure and flexural strength under this interaction. Finally, the model between the deterioration of the flexural strength of pavement concrete and the evolution of microstructures was established.

2. Materials and methods

2.1. Materials

The cement selected in this study is P.O 42.5R Portland cement with a density of 3112 kg/m^3. Its chemical composition is listed in Table 1. Fly ash with a specific area of 270 m^2/kg produced by Datang Hangcheng Co. Ltd. and mineral powder with a specific area of 560 m^2/kg produced by Yaozhou Co. Ltd. were both added to improve the performance of the concrete pavement.

According to the standard [21], the coarse aggregates were obtained from Fuping in northwest China. Crushed limestone with grain sizes ranging from 4.75 mm to 19 mm was used as coarse aggregates. Main properties of the coarse aggregates are listed in Table 2. Fine aggregates with a density of 2650 kg/m^3 were obtained from Ba Bridge, Shaanxi.

A high-performance superplasticizer (KDSP-1) produced by Shanxi Kaidi Building Materials Co. Ltd. was used as water reducing agent. The rate of water reduction can be as high as 26%, the gas content can reach 5%, and the recommended dosage is approximately 0.8–1.2%.

2.2. Mix proportion design

The mix designation of concrete (C40) can be carried out in accordance with the standard [22]. In order for the road concrete to have excellent mechanical properties and durability, the mixture must be optimized. An orthogonal $L_9(3^4)$ test was adopted here to optimize pavement concrete. The adopted slump, flexural strength (f_f), compressive strength (f_c), and the relative dynamic elastic modulus after 200 freeze–thaw cycles (D200) were as optimization indicators. The experimental plans and results are shown in Table 3.

The results of the orthogonal pavement concrete test were analyzed using the range analysis method, and the influence of the water to binder ratios, water reducing to binder ratios, admixture content and unit cement dosage on the workability, as well as the mechanical properties and durability of the pavement concrete, were determined. The optimization results are shown in Table 4.

All mixtures were cast in a mold with dimensions of 100 mm × 100 mm × 400 mm consolidated by a vibrating table and trowel finished. All samples were demolded after 24 h and cured for 90 days under a temperature of 20 ± 2 °C and relative humidity of approximately 95%. After curing, interaction tests were carried out.

2.3. Test methods

2.3.1. Interaction test

The freeze–thaw cycle in seasonal frozen regions usually takes a longer period, and the effect on the cement pavement is time-dependent. Both the role of traffic load on the pavement and effect on the cement pavement are instantaneous [23]. That means the relationship between freeze–thaw and fatigue load is not a complete coupling relationship but an interaction. Thus, the interaction of traffic load and the freeze–thaw cycles was simulated in this investigation.

Fatigue loading was completed by MTS-810, and the effects of ordinary traffic and heavy traffic on cement pavements were simulated by 0.5 and 0.8 of the ultimate load of concrete, respectively [24]. A three-point sine wave function with a loading frequency of 10 Hz and a 0.1 ratio between the low stress and high stress was adopted to simulate vehicle driving on the road [25]. The freeze–thaw test was carried out in accordance with the Chinese Standard GB/T 50082-2009 [26]. A fast freeze–thaw test device (KDR-III) was used to complete the freeze–thaw cycle. The freezing temperature of concrete ranged from -18 °C to 5 °C. The time for each freeze–thaw cycle was 4 h, which included 2 h for freezing and 2 h for thawing.

According to recommendations in the literature, a four-stage interaction of the fatigue load and freeze–thaw cycle was designed [27]. The interaction test is comprised of 7.2 million fatigue loads and 75 freeze–thaw cycles. Through the preliminary interaction test, it was found that the pavement concrete was destroyed prematurely under the interaction of high stress levels and the freeze–thaw cycle. Therefore, reducing the number of freeze–thaw cycles to 50 in each interaction test avoided excessive destruction of the specimen. At the same time, due to the slow pavement concrete damage in the early stage, the microstructure and strength of the specimens after the first interaction test were not tested. In all, the controlled concrete was defined as stage I, and the specimens after two interaction tests were defined as stage II. Then, the specimens subjected to every interaction test were defined as either stage III and stage IV. The detailed program of the interaction test is shown in Fig. 1 and Table 5.

2.3.2. Flexural strength test

The flexural strength test of pavement concrete was carried out by using a YES-300B tester. According to the standard [28], the loading rate ranged from 0.05 MPa/s to 0.08 MPa/s.

Every group with 3 specimens was tested with fatigue load and freeze–thaw cycle interaction under stress levels of 0.5 (0.5S and

Table 1
Chemical composition of P.O 42.5R.

Composition	C_3S	C_2S	C_3A	C_4AF	f-CaO
W (%)	57.46	21.88	7.03	13.14	0.59

Table 2
Main properties of coarse aggregates.

Items	Density (kg/m^3)	Crushing value (%)	Needle plate (%)	Sediment percentage (%)	Organic content (%)
Test value	2800	7.0	4.5	0.4	0.4

Table 3
Design and results of pavement concrete orthogonal experiment.

No.	Water to binder ratios	Water reducing to binder ratios (%)	Admixture content (%)	Unit cement dosage (kg/m^3)	Test result			
					Slump (mm)	28 d f_f (MPa)	28 d f_c (MPa)	D200 (%)
1	0.37	0.6	15	295	35	6.07	45.3	85
2	0.37	0.8	25	315	45	5.68	41.7	89
3	0.37	1.0	35	335	50	6.43	49.9	86
4	0.34	0.6	25	335	35	6.94	48.2	88
5	0.34	0.8	35	295	30	6.53	46.8	87
6	0.34	1.0	15	315	35	6.61	47.5	85
7	0.31	0.6	35	315	20	6.04	50.2	88
8	0.31	0.8	15	335	25	5.86	43.5	87
9	0.31	1.0	25	295	25	6.12	44.9	91

Table 4
Concrete pavement mix design.

Water to binder ratios (%)	Cement	Powder	Flay ash	Water	Coarse aggregate	Sand	Water reducer
	kg/m^3						
0.34	315	63	42	143	1114	734	2.52

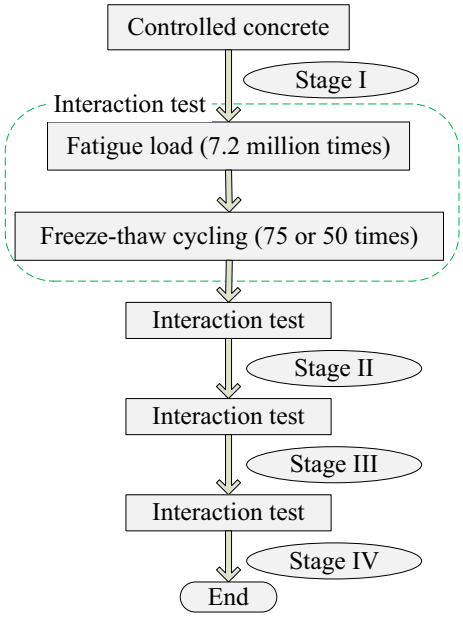

Fig. 1. Flow chart of interaction experiment.

F-T) and 0.8 (0.8S and F-T). After testing, the flexural strength of the specimen was determined, and the average value of the test result was taken as the result.

2.4. Pore structure quantification

2.4.1. Mercury injection test

Vibratory grouting technology was adopted in the construction of concrete pavement, and the pore structure of pavement concrete varies with the slab thickness. To ensure the mercury injection test results are representative, stratified sampling was used in this study. 5 mm × 5 mm × 5 mm slices were obtained from the middle of concrete specimens using a cutting machine, and the sampling location was as shown in Fig. 2. After sampling, the surface of each slice was cleaned with anhydrous ethanol, and then the slices were dried in an oven.

Porosity is the ratio of the pore volume to the concrete volume, and it can reflect the concrete density. The specific surface area (SSA) is the total area of the internal pores per unit mass of material, which can reflect the pore size distribution in the case of the same porosity. The average pore diameter (APD) and area middle aperture (AMA) can reflect the pore size from the diameter and area of pores, respectively. The pore parameters and pore size distribution of pavement concrete were measured by an AutoPore IV 9510 mercury porosimeter, from the Northwest Research Institute of Chemical Industry. The first mercury injection and mercury removal were performed to obtain a mercury injection curve and mercury removal curve after the slices were evacuated. Then, secondary mercury injection was performed to obtain the porosity and pore size distribution (PZD), and SSA, APD, AMA and most probable aperture (MPA) were obtained by data processing.

Table 5
Test scheme of fatigue load and freeze–thaw interaction.

Interaction phase	Stress level of 0.5		Stress level of 0.8	
	Fatigue load (million times)	Freeze-thaw cycles (times)	Fatigue load (million times)	Freeze-thaw cycles (times)
I	0	0	0	0
II	14.4	75	14.4	50
III	21.6	150	21.6	100
IV	28.8	225	28.8	150

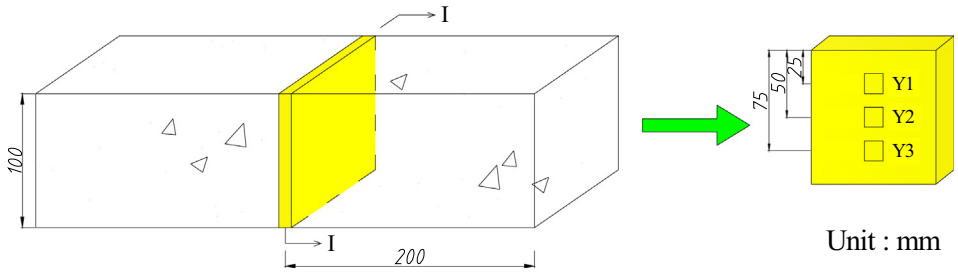

Fig. 2. Sampling locations of the mercury injection test.

2.4.2. Optical microscopy test

The pore spacing factor (PSF) is the distance between bubble centers, and it can reflect the ability of pores to diffuse internal stresses in concrete structures. Stomatal structure parameters were measured by a digital stereomicroscope (SZ-DM200, Chongqing Ott Optical Instrument Co., Ltd.). 1-cm-thick slices were obtained from the middle of concrete specimens, and the surface of the slices were cleaned with anhydrous ethanol. Abrasive papers with grits from #200 to #1000 were used to polish the slices. A polishing machine with chromium oxide was adopted to polish the slice surfaces, and then the slices were cleaned and dried. PSF could be calculated by the length and quantity of stoma according to the standard [22].

3. Results and discussion

3.1. Flexural strength

The flexural strength result is illustrated in Fig. 3. The flexural strength of concrete under interaction showed a parabolic attenuation trend. Compared with the initial flexural strength, the flexural strength of pavement concrete decayed by 0.29 MPa (stage II), 0.68 MPa (stage III) and 2 MPa (stage IV) under the interaction of the 0.5 stress level and the freeze–thaw cycles. Meanwhile, the flexural strength of pavement concrete decayed by 0.56 MPa (stage II), 1.22 MPa (stage III) and 3.13 MPa (stage IV) under the interaction of the 0.8 stress level and the freeze–thaw cycles. Clearly, the flexural strength attenuation of concrete was not significant in the early stage. With the increase in interaction times, the deterioration of the flexural strength gradually increased until the service life of the pavement concrete was seriously affected because the flexural strength was greatly reduced at the late stage.

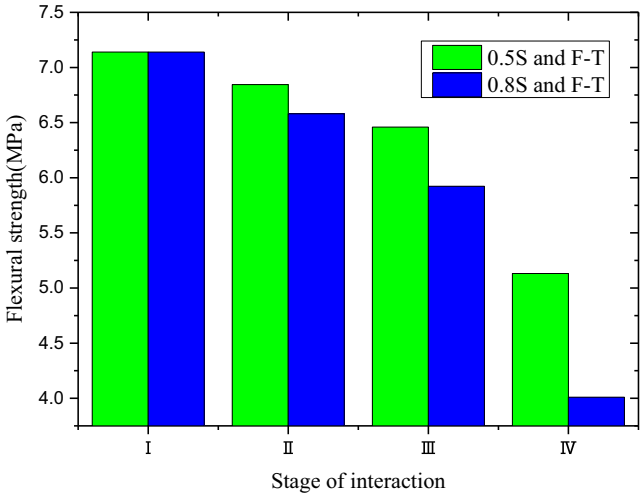

Fig. 3. Flexural strength of concrete under different interactions.

Compared with the interaction under different stress levels, the flexural strength with interaction under a stress level of 0.8 is lower than that with interaction under a stress level of 0.5, respectively, by 4% (stage II), 8.3% (stage III) and 21.8% (stage IV). This suggests that the higher stress level will accelerate the concrete flexural strength attenuation. In particular, the interaction of heavy traffic and freeze–thaw cycles will considerably deteriorate the flexural strength of pavement concrete at the late stage of interaction.

3.2. Characteristic parameters of pore structure

Specimens subjected to the interaction were sampled for pore structure testing. The average values of the pore characteristic parameters of different sampling locations were used as the pore structure test results of the whole specimen, as shown in Fig. 4.

In Fig. 4(a), the porosity inside the pavement concrete with different interactions decreases first and then increases, and the porosity at the 0.8 stress level is greater than that at the 0.5 load level. Compared with the initial porosity of pavement concrete, the porosity in stage II is reduced by 55.5% (0.5 stress level) and 38.9% (0.8 stress level). It is suggested that the porosity decreases and the compactness increases in the early stage of interaction. Then, the porosity increases and the internal density decreases continuously with the increase in the interaction phase. It can be seen that the loading stress and the crystallization expansion of the freeze–thaw cycle promote the development of pores and accelerate the pore structure damage.

In Fig. 4(b), the change trend of the specific surface area is composed of two parabolas, which are gradually transited from a concave parabola to a convex parabola. Before the first turning point, the specific surface area was reduced and was then increased between the first and second turning points; finally, the specific surface area decreased after the second turning point. This result was caused by the composite effect of pore over-compression and the splitting effect. Comparing the specific surface area under the interaction of different stress levels, it differs by 0.8% (stage II), 5.6% (stage III) and 2.3% (stage IV) between the 0.5 stress level and the 0.8 stress level. Little attenuation difference occurs for the specific surface area under the interaction of different stress levels.

As presented in Fig. 4(c) and (d), the average pore diameter and area middle aperture have similar patterns of change, both increasing first and then decreasing. This means that in the early stages of interaction, the pores in the concrete are constantly coarsening. Combined with the porosity change, this is due to the load effect and the freeze–thaw effect on the compression of small pores and expansion of large pores, resulting in the overall increase in pore diameter. Then, the expansion and deformation of the large pores reached the limit and the split occurred, resulting in an overall decrease in number of pores. After stage II, the average pore diameter and area middle aperture continuously decrease, showing that the interior pores of the pavement concrete continue to refine after considerable fatigue loading and freeze–thaw

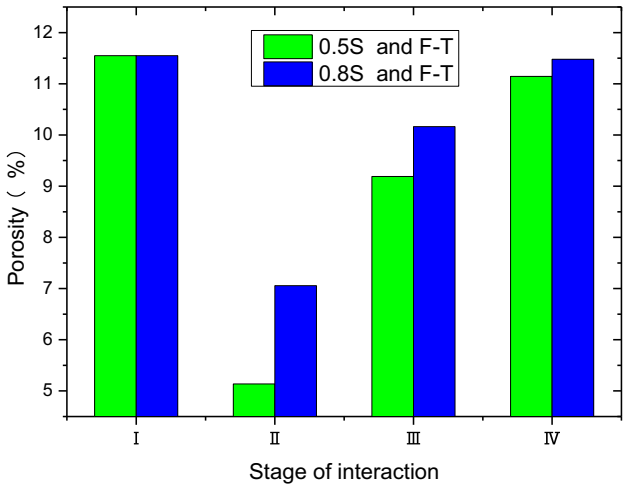

(a) Porosity

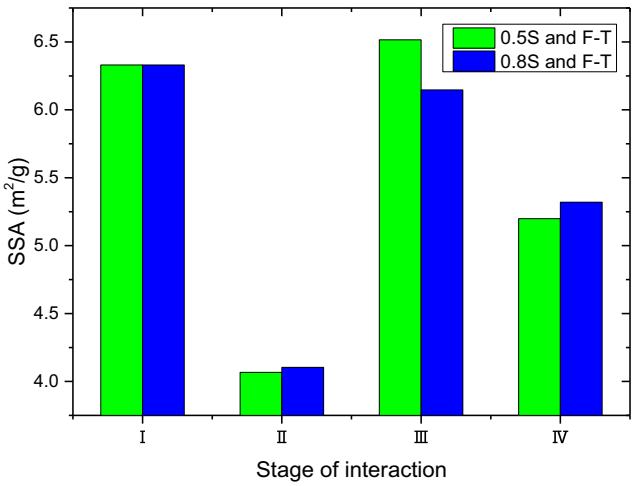

(b) Specific surface area

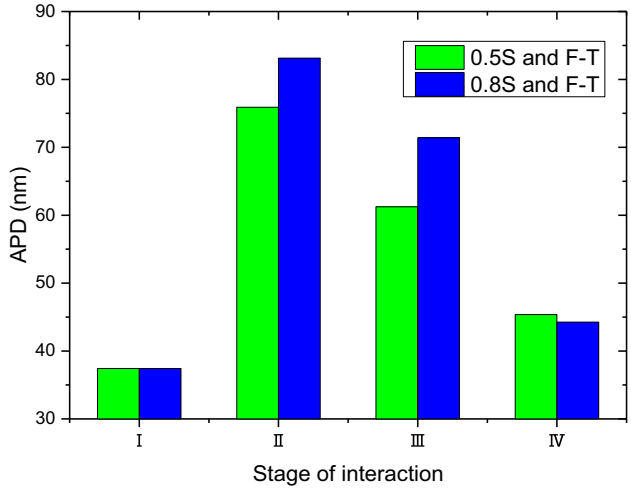

(c) Average pore diameter

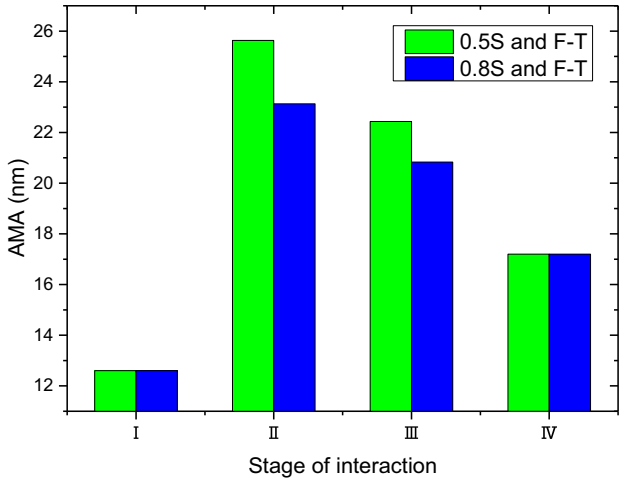

(d) Area middle aperture

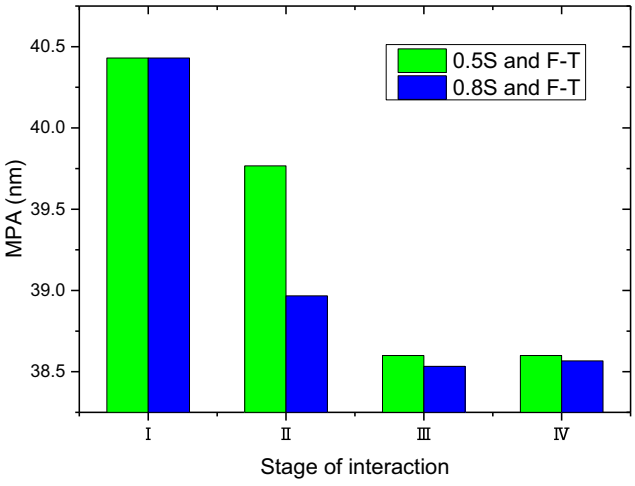

(e) Most probable aperture

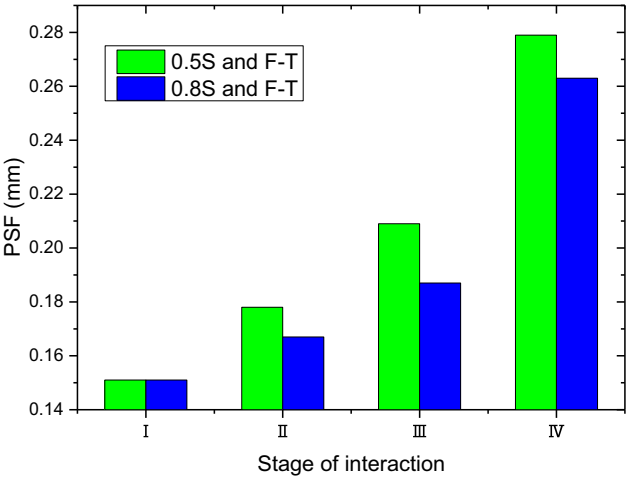

(f) Pore spacing factor

Fig. 4. Variation in characteristic parameters of concrete pavement under different interactions.

interaction. In Fig. 4(e), the most probable aperture slightly decreases and then tends to be 38.6 nm, which shows that the effect of interaction on the most probable aperture is not significant.

The pore spacing factor of pavement concrete increases with the increase in interaction, and the growth trend is approximately exponential, as shown in Fig. 4(f). The hole spacing factor increases by 17.8% (stage II), 38.4% (stage III) and 84.8% (stage IV) under interaction of the 0.5 stress level. When the test condition is under interaction of the 0.8 stress level, the hole spacing factor increases by 10.6% (stage II), 23.8% (stage III) and 74.5% (stage IV). The increase in the pore spacing factor indicates frost resistance attenuation of pavement concrete after interaction. In particular, the pore spacing factor of stage IV of interaction is as high as 0.279 mm (0.5 stress level) and 0.263 mm (0.8 stress level), which show that the frost resistance of pavement concrete is seriously attenuated. Comparing the pore spacing factor under the interaction of different stress levels, it can be found that the pore spacing factor under the interaction of the 0.5 stress level is larger than under the 0.8 stress level. This is because the low stress level corresponds to more freeze–thaw times in the design of the scheme, indicating that the effect of the freeze–thaw action on the pore spacing factor is more significant than that of the load.

3.3. Pore size distribution

The pores inside the concrete are divided into harmless pores (aperture smaller than 20 nm), less harmful pores (aperture range from 20 nm to 50 nm), harmful pores (aperture range from 50 nm to 200 nm) and more harmful pores (aperture larger than 200 nm) according to the aperture division principle by Wu ZW [29]. The average value of the pore size distribution in different sampling positions is used as the pore size distribution of the specimens under interaction, as shown in Figs. 5 and 6. From the figure it can be seen that the harmless pores gradually disappear, and the more harmful pores increase. There are small changes of less harmful pores and harmful pores.

Combining the pore size distribution analysis with the change rules of the pore characteristic parameters under the interaction, it is clear that some of the small pores are compressed, and big pores expand in the early stage of interaction. As a result, the proportion of harmless pores is reduced by compression, and harmful pores expand into more harmful pores. In this stage, the total pore volume in the pavement concrete decreases, and the porosity

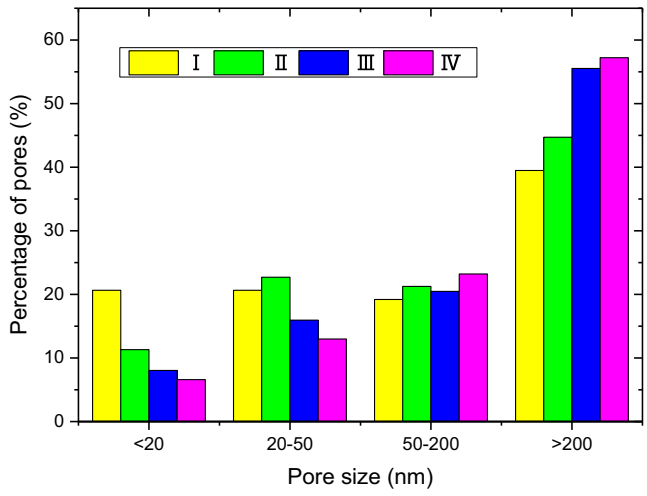

Fig. 5. Variation in pore size distribution in pavement under interaction at the 0.5 level.

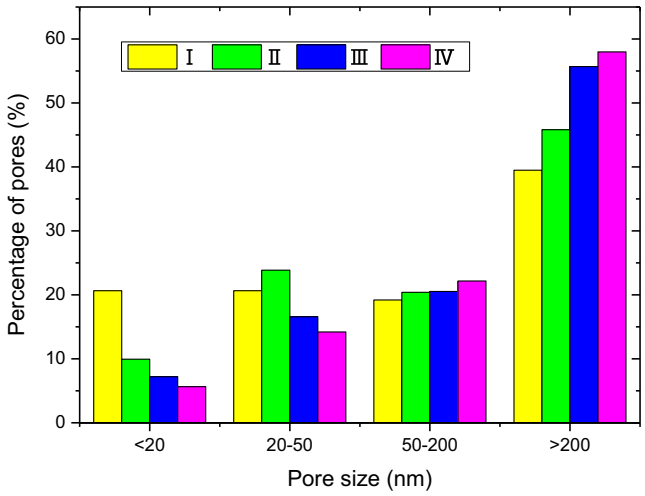

Fig. 6. Variation in pore size distribution in pavement under interaction at the 0.8 level.

decreases. The increase in the interaction results in higher concrete porosity and the presence of more harmful pores. When the expansion deformation of big pores reaches the limit, the pores will split into small pores and cause an increase in the proportion of harmful pores.

3.4. Pore structure deterioration mechanism

Fig. 7 illustrates the deterioration process of the pore structure under different stages of interaction. Fig. 7(a) shows that there are many different kinds of pores in pavement concrete after interaction. A crack with a width of approximately 4 mm is generated around the pore. Fig. 7(b) shows that the pores continue to increase, an obvious crack appears in the pores density, and original cracks expand in both length and width. Further, a vertical microcrack occurs in the middle of the original crack under interaction of fatigue load and freeze–thaw cycling. In stage IV of interaction, as shown in Fig. 7(c), the set cement becomes loose, while the pore expands and gradually connects. A large number of microcracks can be seen inside the matrix and the interface transition zone. As the interaction proceeds, the cracks continuously expand and penetrate to form cross cracks, causing serious damage to the internal structure. The expansion and contraction stresses caused by the freeze–thaw cycle as well as the load stress may cause these results. Thus, the complex stress on the concrete pavement leads to pore structure deterioration, resulting in the generation of a large number of new cracks.

4. Correlation analysis of flexural strength and pore structure

4.1. Gray relational analysis

The gray relational analysis (GRA) results in essential contents of the gray system theory formulated by Deng Julong [30]. The word “gray” here means poor, incomplete, uncertain, etc. It can be used to look for the link in an unknown system through limited data. In this paper, there are many parameters that can characterize pores but less data of each parameter. To reflect the significant effect of different pore parameters on the macroscopic performance, GRA has been adopted to discuss the influence of different pore parameters on the flexural strength of pavement concrete [31,32].

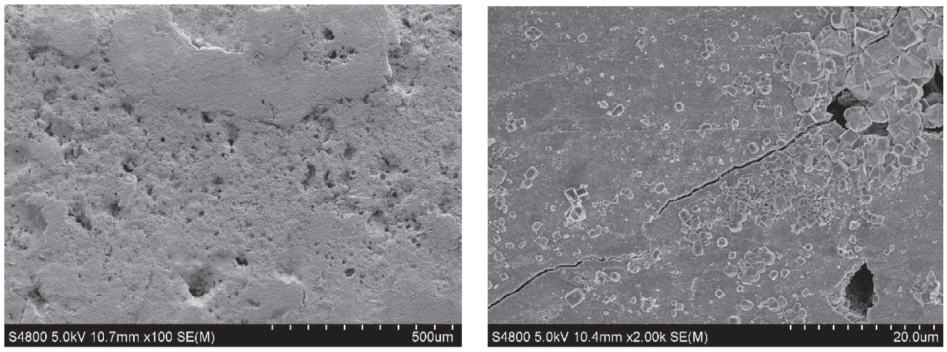

(a) stage II of interaction

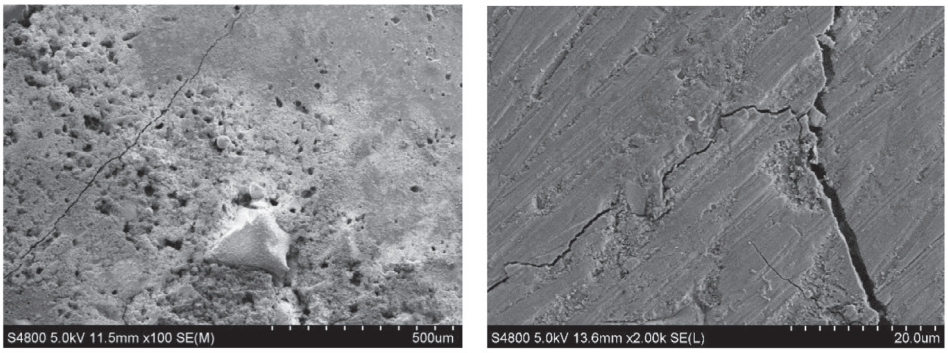

(b) stage III of interaction

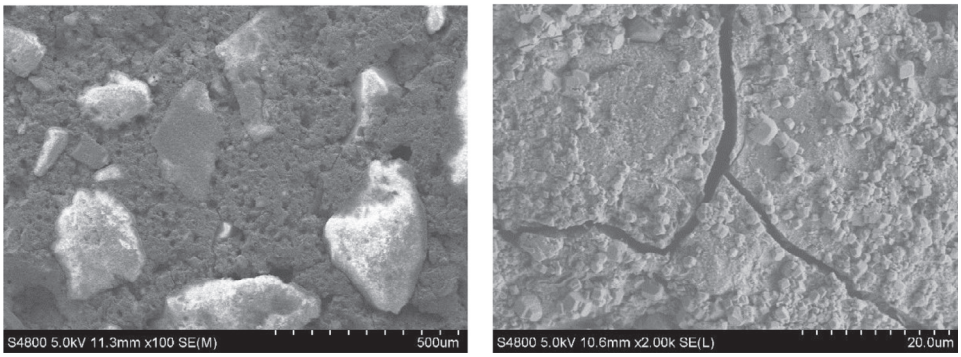

(c) stage IV of interaction

Fig. 7. Microstructure of concrete specimens under different stages of interaction.

The flexural strength under interaction as the original reference sequence represented by $Y(k)$, the pore characteristics parameters and the pore size distribution are used as the comparability sequence represented by $X_i(k)$. Their absolute difference at point k is denoted by $\Delta_i(k)$,where $i = 1, 2, ..., m$; $k = 1, 2, ...n$. Based on the output parameter value desired, Eq. (1) was used for normalizing the experimental data.

$$\begin{aligned} X'_i(k) &= X_i(k)/X_i(1) \\ Y'(k) &= Y(k)/Y(1) \end{aligned} \tag{1}$$

After normalizing, the gray coefficient at point k is calculated using Eq. (2).

$$\gamma_i(k) = \frac{\Delta_{\min} + \xi \cdot \Delta_{\max}}{\Delta_i(k) + \xi \cdot \Delta_{\max}} \tag{2}$$

where $\Delta_{\min} = \min_i \min_k \Delta_i(k)$, $\Delta_{\max} = \max_i \max_k \Delta_i(k)$, and $\xi \in [0, 1]$ is the distinguishing coefficient and is chosen as $\xi = 0.5$ in this paper.

Then, the gray grade is obtained from Eq. (3).

$$\gamma_i = \frac{1}{n}\sum_{k=1}^{n}\gamma_i(k) \tag{3}$$

where the gray grade γ_i represents a numerical measurement of the correlation between the reference sequence and the comparability sequence. The more coincidental the two sequences are, the closer the value of the gray grade is to 1.

4.2 Regression analysis based on gray theory

Concrete strength is determined by its internal microstructure, the essence of the deterioration of the flexural strength of pave-

Table 6
Gray correlation degree between flexural strength and pore characteristic parameters under interaction.

Stress level	Porosity	SSA	AMA	APD	MPA	PSF
0.5	0.7643	0.8264	0.5507	0.5788	0.8960	0.6487
0.8	0.8013	0.8062	0.5759	0.5552	0.8507	0.6870

Table 7
Gray correlation degree between flexural strength and pore size distribution under interaction.

Stress level	<20 nm	20 nm–50 nm	50 nm–200 nm	>200 nm
0.5	0.6716	0.8687	0.7768	0.6830
0.8	0.7158	0.8834	0.7692	0.6693

ment concrete under the interaction of fatigue loading; freeze–thaw is the damage evolution of the microstructure [6,33]. There are many parameters that characterize the pore structure of concrete, which reflect the internal defects of concrete structures in different aspects and affect the flexural strength of concrete to a certain extent. The calculation results of GRA are shown in Tables 6 and 7.

It can be seen from Table 6 that the correlation between the most probable aperture and the flexural strength is the highest, and the gray correlation is above 0.85. The correlations between the flexural strength and the pore parameters of the interaction of different stress levels are basically similar. Under the interaction of the 0.5 stress level, the order of correlation is the most probable aperture > specific surface area > effective porosity > pore spacing factor > average pore diameter > area middle aperture. While under the interaction of the 0.8 stress level, the correlation of area median aperture is higher than the average pore diameter.

It can be seen from Table 7 that the correlation between the flexural strength and pore size distribution under interaction of different stress levels are different. The order of correlation is less harmful pores > harmful pores > more harmful pores > harmless pores under interaction of the 0.5 stress level, while the order of correlation is less harmful pores > harmful pores > harmless pores > more harmful pores under interaction of the 0.8 stress level. The correlation between flexural strength and less harmful pores is highest, and the gray correlation is above 0.85. The conclusion is that the less harmful pores have a significant effect on flexural strength.

It can be seen that the gray correlation of the most probable aperture, specific surface area, or the less harmful pores and flexural strength reach 0.8 or greater under the interaction through the above analysis. At the same time, some research results show that the porosity has an important influence on the strength [34–36]. Therefore, the porosity and most probable aperture, specific surface area and less harmful pores are adopted as influence factors of flexural strength. The regression analysis result of flexural strength and microstructure under interaction through SPSS is as follows:

$$\frac{f}{f_0} = -0.410\frac{P_p}{P_{p0}} + 0.395\frac{S}{S_0} + 0.660\frac{P_s}{P_{S0}} + 2.349\frac{P_M}{P_{M0}} - 2.002$$
$$R^2 = 0.877 \quad (4)$$

where f, P_p, S, P_s, P_M are respectively the flexural strength, porosity, less harmful pore, specific surface area and the most probable aperture after interaction; f_0, P_{p0}, S_0, P_{S0}, P_{M0} are respectively flexural strength, porosity, less harmful pore, specific surface area and the most probable aperture before interaction.

It can be seen from the regression results that there is a negative correlation between the porosity and loss of flexural strength, while the correlation between the less harmful pores, the specific surface area or the most probable aperture and the flexural strength are positively correlated. Furthermore, the regression coefficient R^2 reaches 0.877, showing that there is a good linear relationship between the flexural strength loss and the pore structure evolution under the interaction.

5. Conclusion

In this paper, the deterioration mechanism of concrete pore structure under the interaction of fatigue loading and freeze–thaw with different stress levels has been tested. Pore structure characteristic parameters, pore size distribution and a correlation analysis of flexural strength and pore structure were discussed. The following concluding conclusions can be drawn:

(a) The flexural strength of pavement concrete shows a parabolic attenuation trend under the interaction of fatigue load and the freeze–thaw cycle. As the load stress level increases, the degree of concrete deterioration deepens. The concrete strength decreased by 28.1% (0.5 stress level) and 43.8% (0.8 stress level) in stage IV of interaction, respectively.
(b) The porosity inside pavement concrete under interaction decreases first and then increases, and the greater of load stress level is, the larger the porosity. However, there is not much attenuation difference of the specific surface area under the interaction of different stress levels, and the effect of interaction on the most probable aperture is not significant. At stage IV of interaction, the pore spacing factor reached 0.276 mm (0.5 stress level) and 0.263 mm (0.8 stress level), indication that the frost resistance of pavement concrete is seriously reduced. The effect of the freeze–thaw action on the pore spacing factor is more significant than that of the load.
(c) The more harmful pores increase continuously, while the harmless pores decrease under the interaction. Cracks are generated with the pore structure deterioration. As the interaction proceeds, the set cement becomes loose, while the pores expand and gradually connect. A large number of microcracks can be seen inside the matrix and the interface transition zone, causing serious damage to the internal structure.
(d) The gray correlation of the most probable aperture, specific surface area, and less harmful pores and flexural strength reach 0.8 or more, which were the most important microstructures affecting the flexural strength. There is a good linear relationship between the flexural strength and pore structure under the interaction.

The current study investigated the deterioration process of micropores under interaction. Cracks and the interface transition

zone are important factors affecting the deterioration of the flexural strength of concrete. Therefore, a model containing the three factors, which can be used to predict concrete damage needs to be further investigated.

Conflict of interest

None.

Acknowledgements

This study was financially supported by the National Natural Science Foundation of China (Grant No. 51278059) and the National Science Foundation of Young Scientists of China (Grant No. 5160080049). The authors would like to thank the reviewers of this paper for their comments and suggestions.

References

[1] Y. Qiao, W. Sun, J. Jiang, Damage process of concrete subjected to coupling fatigue load and freeze/thaw cycles, Constr. Build. Mater. 93 (2015) 806–811.
[2] J. Tian, W. Wang, Y. Du, Damage behaviors of self-compacting concrete and prediction model under coupling effect of salt freeze-thaw and flexural load, Constr. Build. Mater. 119 (2016) 241–250.
[3] A.R. Chen, Z.C. Pan, M.A. Ru-Jin, D.L. Wang, New development of mesoscopic research on durability performance of structural concrete in bridges, China J. Highway Transport 29 (11) (2016) 42–48.
[4] W. Li, W. Sun, J. Jiang, Damage of concrete experiencing flexural fatigue load and closed freeze/thaw cycles simultaneously, Constr. Build. Mater. 25 (5) (2011) 2604–2610.
[5] S. Chen Y. Luo Tan Y. Analysison Freeze thawing fault of cement concrete pavementin airport of frozen regions in China Urban Road. Bridg. Flood Control 2013
[6] B.B. Das, B. Kondraivendhan, Implication of pore size distribution parameters on compressive strength, permeability and hydraulic diffusivity of concrete, Constr. Build. Mater. 28 (1) (2012) 382–386.
[7] J. Endawati, Rochaeti, R. Utami, Optimization of concrete porous mix using slag as substitute material for cement and aggregates, Appl. Mech. Mater. 865 (2017) 282–288.
[8] H.L. Wang, C.L. Guo, X.Y. Sun, W.L. Jin, Degradation mesomechanism of concrete deteriorated by soft water, J. Zhejiang Univ. 46 (10) (2012). 1887-92 +922.
[9] O. Deo, N. Neithalath, Compressive behavior of pervious concretes and a quantification of the influence of random pore structure features, Mater. Sci. Eng., A 528 (1) (2010) 402–412.
[10] S.P. Zhang, D. Min, W.U. Jian-Hua, M.S. Tang, Effect of pore structure on the frost resistance of concrete, J. Wuhan Univ. Technol. 30 (6) (2008) 56–59.
[11] K.B. Park, T. Noguchi, Effects of mixing and curing temperature on the strength development and pore structure of fly ash blended mass concrete, Adv. Mater. Sci. Eng. 2017 (6) (2017) 1–11 (2017-3-20).
[12] E. Berodier, K. Scrivener, Evolution of pore structure in blended systems, Cem. Concr. Res. 73 (2015) 25–35.
[13] X.Y. Wang, K.B. Park, Analysis of compressive strength development of concrete containing high volume fly ash, Constr. Build. Mater. 98 (2015) 810–819.
[14] A.U. Ozturk, B. Baradan, A comparison study of porosity and compressive strength mathematical models with image analysis, Comput. Mater. Sci. 43 (4) (2008) 974–979.
[15] I. Odler, M. Rößler, Investigations on the relationship between porosity, structure and strength of hydrated Portland cement pastes. II. Effect of pore structure and of degree of hydration, Cem. Concr. Res. 15 (3) (1985) 401–410.
[16] R. Kumar, B. Bhattacharjee, Porosity, pore size distribution and in situ strength of concrete, Cem. Concr. Res. 33 (1) (2003) 155–164.
[17] S.B. Zhou, A.Q. Shen, X. Li, G.F. Li, A relationship of mesoscopic pore structure and concrete bending strength, Mater. Res. Innov. 19 (sup10) (2016). S10-100-S10-9.
[18] S. Jin, J. Zhang, S. Han, Fractal analysis of relation between strength and pore structure of hardened mortar, Constr. Build. Mater. 135 (2017) 1–7.
[19] S. Hınıslıoğlu, O.Ü. Bayrak, Optimization of early flexural strength of pavement concrete with silica fume and fly ash by the taguchi method, Civ. Eng. Environ. Syst. 21 (2) (2004) 79–90.
[20] A. Saboori, Application of damage mechanics to describe the behavior of concrete under fatigue and freeze-thaw processes, Dissertations & Theses – Gradworks 29 (1) (2015) 3–22.
[21] E42-2005 J. Test Methods of Aggregate for Highway Engineering China Communications Press, Beijing, 2005 (in Chinese).
[22] F30-2015 J. Technical Specifications for Construction of Highway Cement Concrete Pavements. China Communications Press, Beijing, 2003 (in Chinese).
[23] G. Makusa J. Mácsik G. Holm S. Knutsson Laboratory test study on the effect of freeze–thaw cycles on strength Can. Geotech. J. 2015 53 6
[24] S. Zhou, J. Liang, A. Shen, A strength damage and fatigue life prediction model of pavement cement concrete under loading low-temperature drying conditions, J. Highway Transport. Res. Dev. 11 (2) (2017) 9–13.
[25] S. Goel, S.P. Singh, P. Singh, Flexural fatigue strength and failure probability of Self Compacting Fibre Reinforced Concrete beams, Eng. Struct. 40 (2012) 131–140.
[26] GB/T50082-2009. Chinese Industrial Standard for test methods of long-term performance and durability of ordinary concrete. Ministry of Housing and Urban- Rural Development, Beijing, 2009 (in chinese).
[27] Lappa ES. High strength fibre reinforced concrete: static and fatigue behaviour in bending. Deflection. 2007.
[28] E30-2005 J. Test methods of cement concrete for highway engineering: China Communications Press, Beijing, 2005 (in Chinese).
[29] Y.C. Guo A.Q. Shen H.E. Tian-Qin S.B. Zhou B. Wang Pore structure research on pavement cement concrete subjected to coupling effect of fatigue load and cyclic freeze-thaw in seasonally frozen ground region China J. Highway Transp. 2016
[30] D. Ju-Long, Control problem of grey systems, Syst. Control Lett. 1 (5) (1982) 288–294.
[31] B. Łaźniewska-Piekarczyk, Examining the possibility to estimate the influence of admixtures on pore structure of self-compacting concrete using the air void analyzer, Constr. Build. Mater. 41 (41) (2013) 374–387.
[32] P. Zhang, C. Liu, Q. Li, Application of gray relational analysis for chloride permeability and freeze-thaw resistance of high-performance concrete containing nanoparticles, J. Mater. Civ. Eng. 23 (12) (2011) 1760–1763.
[33] M.H. Zhang, H. Li, Pore structure and chloride permeability of concrete containing nano-particles for pavement, Constr. Build. Mater. 25 (2) (2011) 608–616.
[34] E.P. Kearsley, P.J. Wainwright, The effect of porosity on the strength of foamed concrete, Cem. Concr. Res. 32 (2) (2002) 233–239.
[35] Li Z, Ma H, Tang S. The assessment of porosity in concrete and its influence to service life design of concrete. The International Conference on Performance-Based and Life-Cycle Structural Engineering, 2012.
[36] F. Vodák, K. Trtík, O. Kapicková, Š. Hošková, P. Demo, The effect of temperature on strength – porosity relationship for concrete, Constr. Build. Mater. 18 (7) (2004) 529–534.